Magnetic and transport behavior of Ni-substituted $GdBaCo_2O_{5+\delta}$ perovskite

A. Bharathi,* P. Yasodha, N. Gayathri, A. T. Satya, R. Nagendran, N. Thirumurugan, C. S. Sundar, and Y. Hariharan
Materials Science Division, Indira Gandhi Centre for Atomic Research, Kalpakkam 603102, India
(Received 27 August 2007; revised manuscript received 5 December 2007; published 15 February 2008)

Electrical resistivity, dc magnetization, ac susceptibility, thermopower, and magnetoresistance measurements have been carried out on Ni-substituted $GdBaCo_2O_{5+\delta}$. Structural characterization of the samples was done by x-ray diffraction and results show a systematic variation in the lattice parameters with Ni substitution. Oxygen stoichiometry determined by iodometric titration suggests that oxygen content remains unaltered with Ni substitution. The metal to insulator transition (T_{MIT}), the paramagnetic to ferromagnetic (FM) transition (T_C), and ferromagnetic to antiferromagnetic (AFM) transition (T_N) are altered strongly by Ni substitution. Magnetization and magnetoresistance studies carried out enable determination of magnetic phase diagram which suggests the stabilization of an AFM ground state for low Ni fractions, FM state for high Ni fractions, and a mixed phase at intermediate Ni fractions.

DOI: 10.1103/PhysRevB.77.085113 PACS number(s): 72.80.Ga, 75.47.−m, 75.30.Kz

I. INTRODUCTION

Transition metal oxides with perovskite structure display a wide variety of challenging phenomena including high temperature superconductivity in cuprates, colossal magnetoresistance in manganites, metal-insulator transition in vanadates, etc.[1–5] Among the transition metal oxides, layered cobalt oxides have attracted a great deal of interest because they have unusual electrical properties such as superconductivity in water intercalated $Na_{0.35}CoO_2$,[6] a high thermopower with metallic electrical conduction in Na_xCoO_2[7,8] and a large magnetoresistance in perovskite derived $LaCoO_3$ compounds.[9] Co in these oxide systems has comparable values of intraatomic Coulomb repulsion energy and the crystal field splitting energy. As a result Co can have multiple spin states in a given oxidation state Co^{3+}: the low spin $(t_{2g}^6, e_g^0, S=0)$, the high spin (HS) $(t_{2g}^4, e_g^2, S=2)$, and the intermediate spin (IS) $(t_{2g}^5, e_g^1, S=1)$.[10] The small energy differences between the different spin states enable spin state transitions[11] by thermal fluctuations and small lattice parameter changes. This, in addition with the possibility of different oxidation states for Co (Co^{2+}, Co^{3+}, and Co^{4+}), results in the occurrence of complex properties in cobaltites that make it a challenging system to investigate.[12–15]

More recently, unusual magnetic and electrical transport properties have been reported for oxygen-deficient double layered perovskite $LnBaCo_2O_{5+\delta}$, where Ln represents lanthanide atom.[16–19] These families of compounds possess extremely rich structural, electronic, and magnetic phase diagrams, spin state transitions, and the metal-insulator transitions.[16–25] In these compounds, the oxygen content determines the nominal valence of Co ions, which varies from 3.5+ for $\delta=1$ to 2.5+ for $\delta=0$, and the mean oxidation number of Co is 3 when $\delta=0.5$. These compounds are formed by the stacking sequence $[CoO_2]$ $[BaO]$ $[CoO_2]$ $[LnO_\delta]$ $[CoO_2]$ along the c direction[26] and the cobalt cations occupy two crystallographic sites with two different coordination environments—pyramidal CoO_5 and octahedral CoO_6 (see Fig. 1). It has been proposed that at low temperature, Co^{3+} occupies intermediate spin state ($S=1$) in the pyramidal environment and low spin state ($S=0$) in the octahedral environment.[27] At high temperature, the Co^{3+} in the octahedra attains an $S=2$ spin state after the spin state transition. This picture has been further elaborated for the understanding of single crystalline samples where the oxygen stoichiometry has been varied in the same sample and a variety of properties, viz., resistivity, magnetization, magnetoresistance, thermopower, and Hall effect, has been measured.[26,28,30,31] These results indicate that there is a strong anisotropy in magnetization which leads to the conclusion that Ising chains are formed along the pyramidal chains, which interact ferromagnetically in a narrow temperature region, below which an antiferromagnetic (AFM) order sets in. An alternative picture of the physics of the $LnBaCo_2O_{5.5}$ system considers that the Co^{3+} in both pyramids and octahedra are in the HS/IS spin state, and in this picture, the low temperature insulating phase arises due to an orbital ordering of the e_g orbital in both pyramids and octahedra, which seems to be consistent with structural data obtained from detailed neutron diffraction measurements[32] done across the metal-insulator transition. This orbital ordering seems to also account for the ferromagnetic (FM) to AFM transition seen on lowering the temperature. Based on

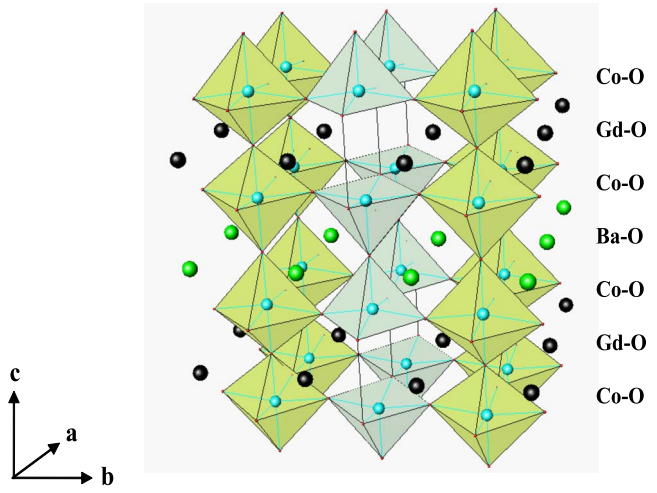

FIG. 1. (Color online) Structure of $GdBaCo_2O_{5.5}$ (from talk by A. Podlesnyak Tashkent Workshop, 2003).

the O isotope effect on the T_{MIT}, it is suggested that the metal-insulator transition (MIT) arises as a consequence of delocalization of holes in the $pd\sigma$ band,[33] which occurs due to a hybridization of the oxygen p and Co e_g level. Electronic structure calculations,[34] are in overall agreement with this picture but disagree on the particular orbital involved in the orbital ordering.

Chemical substitution of $GdBaCo_2O_{5.5}$ system has not been so far investigated. The main objective of this work is to investigate the effect of transport and magnetic behavior of the compound by substituting Ni at the Co crystallographic site without affecting the total oxygen content of the parent compound. It is expected that Ni replacing Co will lead to electron doping. This paper deals with the synthesis of the samples $GdBaCo_{2-x}Ni_xO_{5.5}$ for $x=0.0$ to $x=0.4$. X-ray diffraction (XRD) measurements are used to obtain changes in lattice parameters as a function of Ni substitution at room temperature. Electrical resistivity, thermopower, magnetoresistance and magnetization behavior have been measured in all the samples in the 300–4.2 K temperature range. The samples were characterized for oxygen stoichiometry by iodometric titrations.

II. EXPERIMENTAL DETAILS

Polycrystalline samples of $GdBaCo_{2-x}Ni_xO_{5+\delta}$ with the Ni fractions of $x=0.0$, 0.05, 0.1, 0.2, 0.3, and 0.4 were prepared using conventional solid state reaction method. For all samples indicated stoichiometric mixtures of the starting materials Gd_2O_3, $BaCO_3$, Co_3O_4, and NiO were pressed into pellets. As a first step, decarbonation was carried out at 850 °C for 18 h, followed by grinding, pelletising, and sintering at 1050 °C in air for 30 h. The latter procedure was repeated several times to get homogeneous samples. Scanning electron microscopy measurements revealed a uniform concentration of Co and Ni in all grains with no appearance of second phase particles. Samples were examined by x-ray powder diffraction using a STOE diffractometer with Cu K_α line. ac susceptibility measurements were carried out in a dipstick in the temperature range of 4.2–300 K using a homemade mutual inductance coil. Thermoelectric power measurements were done using exchange gas cryostat in the temperature range of 77–300 K. dc resistivities of the samples both in low temperature (4.2–300 K) and in high temperature (300–500 K) ranges have been measured using van der Pauw four-probe method. Magnetoresistance measurements were carried using a 12 T superconducting magnet in an exchange gas cryostat. The temperature range accessible in the cryostat in fields up to 12 T was 4.2–300 K. Magnetoresistance, ac susceptibility, and thermopower experiments were automated using LABVIEW software.

III. RESULTS

A. Sample characterization

The x-ray diffraction patterns of the samples are shown in Fig. 2. XRD pattern indicates that all the samples have formed single phase for $x \leqslant 0.4$. For $x=0.5$, a small fraction of Gd_2BaNiO_5 forms, which remains even with repeated heat treatments. All the patterns have been indexed to primitive orthorhombic structure with *Pmmm* symmetry. The lattice parameters were obtained in phase pure samples. The inset of Fig. 2 shows the variation of lattice parameters with Ni substitution. It can be seen that the a-lattice parameter decreases monotonically, whereas the b and c parameters show a small increase. The oxygen content of the rare earth cobaltate $GdBaCo_2O_{5+\delta}$ was determined using iodometric titration method in accordance with the results of Conder *et al.*[35] which is tabulated in Table. I. It is clear from the table that the oxygen content remains unaffected by Ni substitution and is very close to 5.5, suggesting that average valence of both Co and Ni in all the samples is close to 3+.

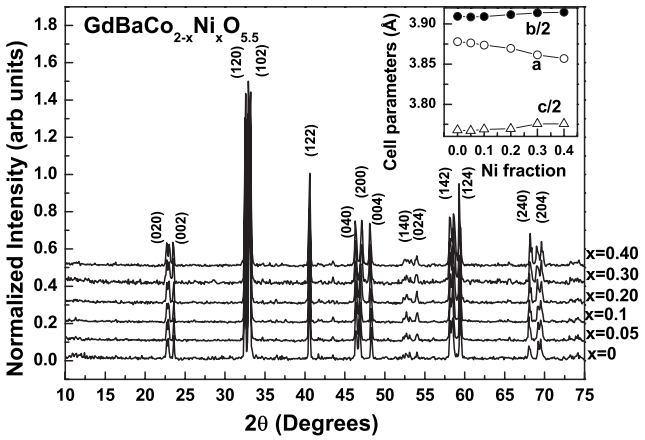

FIG. 2. XRD pattern of $GdBaCo_{2-x}Ni_xO_{5+\delta}$ ($x=0.0$, 05, 0.1, 0.2, 0.3, and 0.4). These patterns are indexed to orthorhombic structure with *Pmmm* symmetry. Intensity for different x has been shifted along the ordinate for clarity. The inset shows the variation of cell parameters a, $b/2$ and $c/2$ with Ni substitution.

B. Magnetization

Field cooled magnetization measurements were carried out in a home built superconducting quantum interference device magnetometer[36] with a perturbing magnetic field of 15 Oe. The magnetization versus temperature curves for the pristine and Ni-substituted samples are shown in Fig. 3. It can be seen from Fig. 3 that with decrease in temperature from 300 K, in the pristine $GdBaCo_2O_{5.5}$, the magnetization shows a precipitous increase at 283 K, followed by a sharp fall at 251 K. This corresponds to the well-known para- to

TABLE I. Oxygen stoichiometry values for different fractions of Ni in $GdBaCo_{2-x}Ni_xO_{5+\delta}$.

Ni fraction	Total oxygen content
0	5.54 ± 0.01
0.05	5.55 ± 0.01
0.1	5.53 ± 0.01
0.2	5.54 ± 0.01
0.3	5.50 ± 0.01
0.4	5.54 ± 0.03

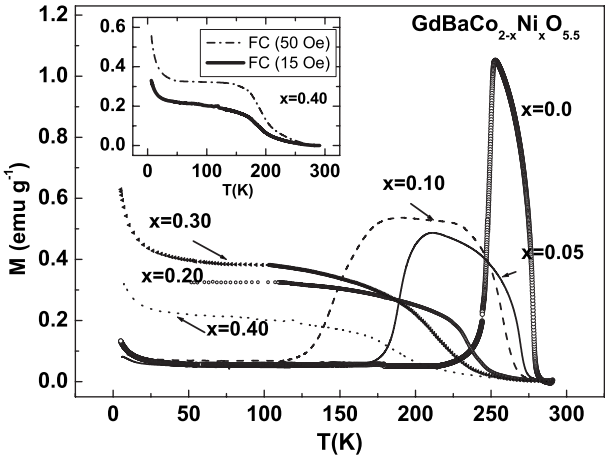

FIG. 3. Field cooled dc magnetization with temperature in $GdBaCo_{2-x}Ni_xO_{5.5}$ for various concentrations of Ni. The field cooled data for 15 and 50 Oe for the $x=0.4$ sample are compared in the inset.

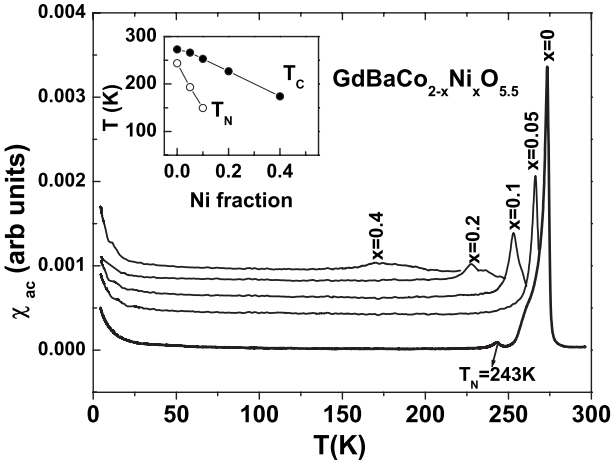

FIG. 4. ac susceptibility variation of $GdBaCo_{2-x}Ni_xO_{5.5}$ for various concentrations of Ni. Curves for different x are shifted along the ordinate for clarity. Inset: variation of T_C and T_N with respect to Ni substitution obtained from magnetization measurements.

ferrotransition (T_C) and ferro- to antiferrotransition (T_N), respectively, seen in the system.[17] With Ni substitution, it can be seen that the transition temperature T_C shifts to lower temperatures and the transitions are significantly broadened. The fall in magnetization that occurs at T_N is seen to show a larger shift with increase in Ni concentration. This transition is also significantly broadened in the samples containing Ni fractions of $x=0.05$ and $x=0.10$. For Ni concentrations of $x=0.20$, $x=0.30$, and $x=0.40$, the magnetization increases at T_C but does not show the fall characteristic of T_N. At very low temperature (<25 K), a rise in the magnetization is observed in all the samples, which is attributed to the paramagnetism of the Gd ions.[30] In the inset of Fig. 3, the magnetization curve is shown for measurement done on the $x=0.4$ sample with fields of 50 and 15 Oe. The measurement done at 50 Oe brings out the flat behavior of $M(T)$ below T_C very clearly. The flat $M(T)$ behavior observed in samples with $x=0.2$, $x=0.3$, and $x=0.4$ indicates that the ferromagnetic phase persists up to 4.2 K. In order to mark the transitions, the derivative of the magnetization plot was obtained: The points at which dM/dT showed a minimum was associated with the T_C and the point at which dM/dT showed a maximum was identified with T_N. For samples with Ni fractions, $x=0.20$, 0.30, and 0.40, only T_C could be identified.

C. ac susceptibility

Figure 4 shows the temperature dependence of ac susceptibility in the temperature range of 4.2–300 K. The pristine sample shows a sharp peak at T_C and small peak is also seen at T_N. It can be seen from Fig. 4 that the peaks associated with ferromagnetic transition become broader with Ni substitution, similar to the observation made in the magnetization experiments (see Fig. 3). No susceptibility signal was observed at the AFM transition in the Ni-substituted samples in our measurements. The peak in the susceptibility corresponds to the point of the fastest rise in the M versus temperature curve, corresponding to T_C. The inset of Fig. 4 shows the variation of T_C and T_N with Ni substitution as obtained from derivative of the M versus T curves (Fig. 3). The T_C obtained from susceptibility measurements are seen to be in good agreement with that obtained from magnetization. It is clear from the inset of Fig. 4 that both T_C and T_N decrease with Ni substitution. It is also clear from the Fig. 4 that at temperatures below 25 K, there is a distinct upturn in the ac susceptibility which arises due to the paramagnetic contribution of the Gd magnetic moment.

D. Thermoelectric power

Figure 5 shows the temperature dependence of the thermoelectric power (TEP) in the temperature range of 77–300 K. From Fig. 5, it can be seen that the room temperature thermopower of the pristine sample is positive and is ~88.2 μV/K. This value in the $x=0.05$ sample is ~105 μV/K, which decreases with further addition of Ni. When $x \geq 0.3$, the room temperature TEP becomes small and

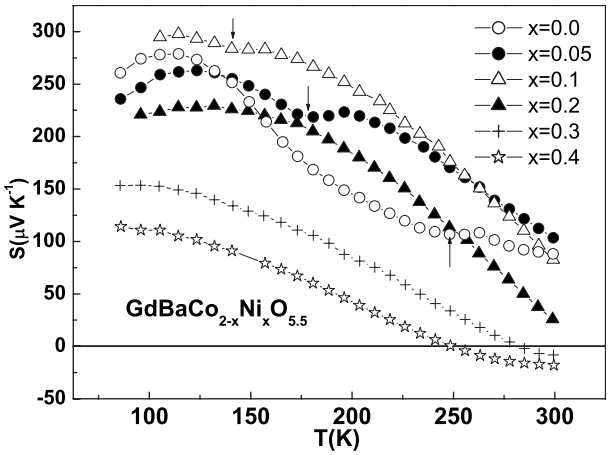

FIG. 5. (a) Thermoelectric power (S) as a function of temperature in Ni-substituted $GdBaCo_2O_{5.5}$ samples. Arrows indicate the antiferromagnetic transition temperature.

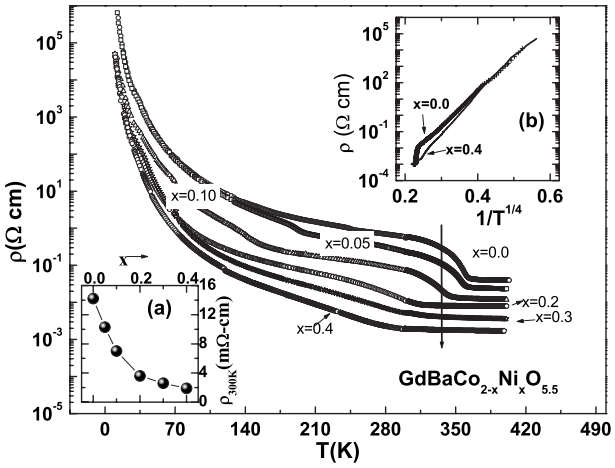

FIG. 6. Temperature dependence of the normalized resistivity of the samples in the temperature range of 10–400 K. Data for different x shifted along the ordinate for clarity. Inset (a): variation of room temperature resistivity with Ni substitution. Inset (b): variation of $\log(\rho)$ versus $1000/T^{(1/4)}$ for $x=0.0$ and $x=0.4$.

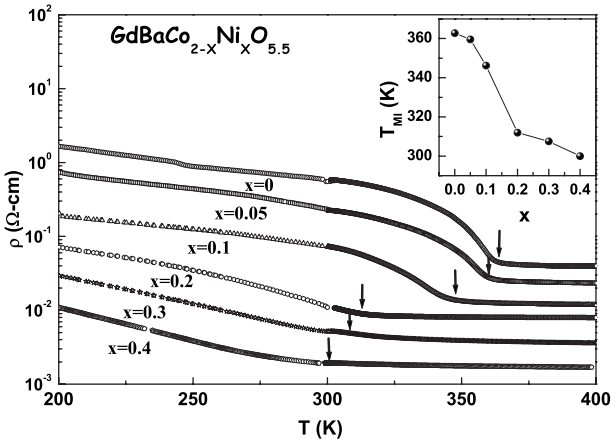

FIG. 7. Expanded view of temperature dependence of resistivity of the samples in the metal-insulator transition region. Data for different Ni concentrations have been shifted along the ordinate for clarity.

negative and is ~ -18 μV/K for a Ni fraction of $x=0.4$. In all samples studied (cf. Fig. 5), thermopower is seen to increase with decrease in temperature, showing a maximum of ~ 300 μV/K for $x=0.1$ at ~ 100 K. Below 100 K, the TEP in all samples shows a tendency to remain constant. The 100 K TEP values have also a tendency to decrease with Ni substitution, showing a value of ~ 100 μV/K for $x=0.40$. A distinctive feature of the thermopower is a small dip marked by the arrows, seen for samples with $x<0.1$. This temperature corresponds to the transition to the antiferromagnetic state as clearly seen from the magnetization curves (cf. Fig. 3). It is to be noted that the above mentioned diplike feature in thermopower is absent in samples that do not undergo an antiferromagnetic transition (cf. Fig. 5). Thus, our thermopower data suggest the occurrence of an anomaly at the antiferromagnetic transition. The signature of the metal-insulator transition is also observable in the TEP data shown in Fig. 5. For samples with Ni fractions $x>0.3$, S goes over to negative values at 280 and 250 K for $x=0.30$ and $x=0.40$, respectively, which is close to the temperature corresponding to the MIT determined by resistivity measurements to be shown later.

E. dc electrical resistivity

Figure 6 shows the temperature dependence of resistivity of the samples in the temperature range of 4.2–400 K. Inset (a) shows the variation of room temperature resistivity of the samples with increasing Ni content. It is clear that the room temperature resistivity decreases systematically with Ni substitution. However, all samples show a temperature dependence corresponding to an insulating behavior, irrespective of the concentration of Ni substituted. The temperature dependent resistivity in all samples shows variable range hopping behavior in the insulating region as evident from the plot $\log(\rho)$ versus $1/T^{1/4}$, as shown in inset (b) of Fig. 6 for select two samples. The arrow in Fig. 6 indicates the sudden drop in the resistivity which is attributed to the MIT, as shown in expanded scale in Fig. 7.The MIT in the parent compound occurs at $T\sim 360$ K, and the magnitude of the resistivity change across the transition is by a factor of 12. With Ni substitution, the magnitude of change in resistivity across the MIT decreases and the transition broadens. In particular, in the sample with Ni fraction of $x=0.40$, the transition is marked only by a change in slope. These transitions were also tracked by differential scanning calorimetry (DSC) measurements,[37] where again it could be inferred that transition broadens with increase in Ni content. The variation of T_{MIT} with Ni concentration obtained from the resistivity data is shown in the inset of Fig. 7.

F. Magnetoresistance

Figures 8(a)–8(e) are the compared temperature dependence of resistivity under applied magnetic fields of 0, 6, and 9 T for Ni fractions of $x=0.0$, 0.05, 0.10, 0.20, and 0.30. The corresponding magnetoresistance (MR) defined as $[R(H,T)-R(0,T)]/[R(0,T)]$ expressed in percentage is shown in Figs. 8(f)–8(j), respectively. It is clear from the figure that a marked negative magentoresistance is observed in samples with Ni fractions, $x=0.0$, $x=0.05$, and $x=0.10$. Compared with the magnetization data shown in Fig. 3, it can be seen that MR shown in Figs. 8(f) and 8(h) builds up at T_N for these samples. In contrast in the $x=0.20$ sample [Fig. 8(i)], it is seen that a finite negative MR builds up gradually with decrease in temperature to a value of 30% at 50 K at an applied field of 9 T. This value is much smaller than the MR observed in $x=0.10$ sample [cf. Figs. 8(c) and 8(h)]. For a higher Ni fraction of $x=0.30$, shown in Figs. 8(e) and 8(j), the MR is smaller and is $\sim 10\%$ at 50 K under 9 T. However, in the $x=0.40$ sample (not shown in figure), practically, no MR was observed. From our data in Fig. 8, we see that maximum MR for a given field is seen in the sample containing a Ni fraction of $x=0.10$. In the $x=0.20$ and 0.30 samples, eventhough the magnetization data suggest a ferromagnetic behavior, a fairly large MR is observed in these

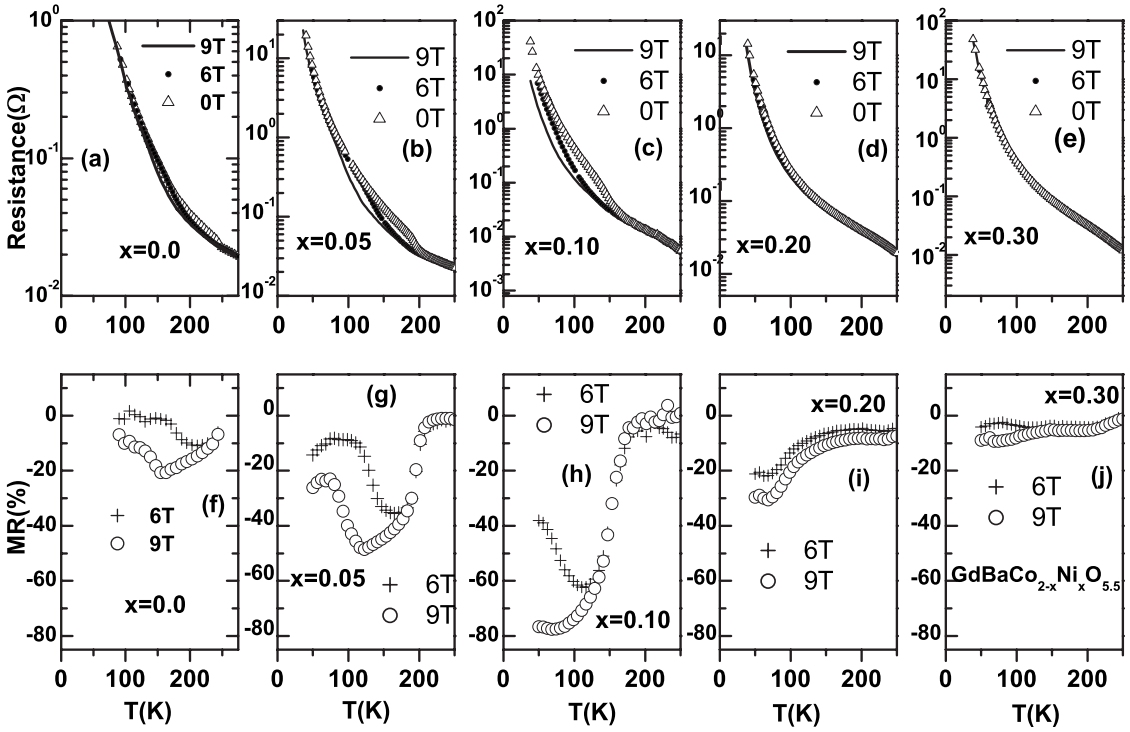

FIG. 8. [(a)–(e)] Temperature dependence of resistivity for $GdBaCo_{2-x}Ni_xO_{5.5}$ for $x=0.0$, $x=0.05$, $x=0.10$, $x=0.20$, and $x=0.30$ with external magnetic fields of 9, 6, and 0 T (without) magnetic field in the temperature range of 4.2–300 K. (f)–(j): the corresponding magnetoresistance evaluated using the formula $[R(H,T)-R(0,T)]/[R(0,T)]$ for $H=9$ and 6 T, expressed in percentage.

samples. To illustrate the increase in the magnitude of observed MR with Ni substitution, we compare MR versus magnetic field in the pristine sample and the $x=0.10$ sample at different temperatures in Fig. 9. It is clear from the figure that the magnitude of MR in the $x=0.10$ sample is much larger than that observed for polycrystalline $GdBaCo_2O_{5.5}$. Further, it is also apparent from the figure that the MR increases rapidly at lower fields in the Ni substituted as compared to that in the pristine sample and the MR variation in the Ni-substituted sample field flattens at large magnetic fields. This implies that the antiferromagnetic to ferromagnetic transformation with applied magnetic field is aided by Ni substitution.

IV. DISCUSSION

In this paper, we have presented the results of structural, magnetization, and transport measurements in the $GdBaCo_{2-x}Ni_xO_{5.5}$ system. Here, we consolidate the study and look for some consistencies. At first, we examine structure: The systematic variation in the lattice parameters extracted from the XRD data and the absence of any impurity phases clearly indicates that Ni substitutes at Co site in $GdBaCo_2O_{5.5}$. With Ni substitution a systematic increase in orthorhombicity defined as $(b/2-a)/(b/2+a)$ is seen [see Fig. 10(a)], which arises as a consequence of the decrease in a-lattice parameter and increase in b-lattice parameter (cf. Fig. 2). The variations of the observed orthorhombicity and that of T_{MIT} with Ni substitution are compared in Fig. 10. The figure brings out an interesting one to one correlation between the two, suggesting that the structural change with Ni substitution could be responsible for the observed decrease in T_{MIT}. It is worth pointing out that similar changes in the lattice constants and orthorhombicity were also observed as a function of temperature in $HoBaCo_2O_{5.5}$ system, where a distortion of the CoO_5 pyramids and octahedra[31]

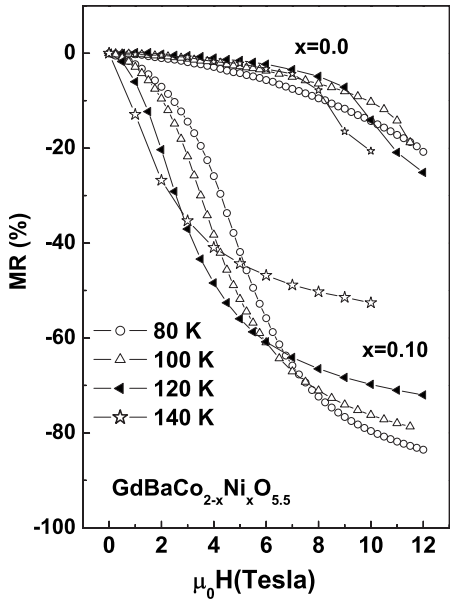

FIG. 9. The variation of magnetoresistance as a function of magnetic field for different temperatures for the pristine sample and that containing a Ni fraction of $x=0.10$.

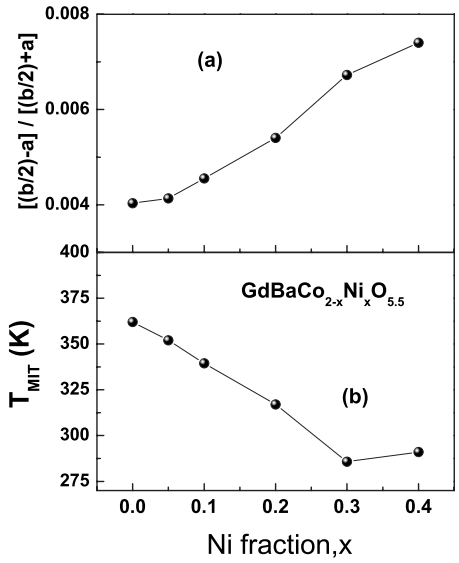

FIG. 10. The variation of the (a) T_{MIT} (b) orthorhombic distortion as a function of Ni concentration. Solid lines are guide for the eyes.

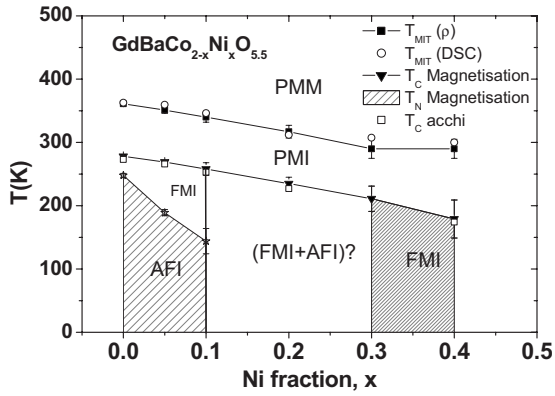

FIG. 11. The phase diagram for $GdBaCo_{2-x}Ni_xO_{5.5}$ as determined from this work. T_{MIT} determined from DSC (Ref. 37) is also shown. PMM—paramagnetic metal, PMI—paramgnetic insulator, FMI—ferromagnetic insulator, and AFI—antiferromagnetic insulator.

enables the spin state transition of the Co^{3+} in the octahedra, giving rise to the MIT. Taking cue from these studies,[31] it can be stated that the observed structural change with Ni substitution could result in the modification of the crystal field energies and consequently the energy required for the spin state transition, which can qualitatively account for the observed decrease in the T_{MIT} with Ni substitution.

From our resistivity data, it is clear that even though there is marginal decrease in the resistivities in the sample due to Ni substitution in the vicinity of the MIT, at low temperatures, the pristine sample and the Ni-substituted sample have similar resistivity behaviors (see Figs. 6 and 7). This brings up an interesting point that even though extra electrons are added to the e_g level by Ni substitution, it does not initiate a metallization in the Co-O_6 network. The extra e_g electrons set into the system by Ni substitution, however, seem to aid the stabilization of a ferromagnetic phase. Another puzzling feature is the observation of large positive thermopower at 100 K in the entire range of Ni concentration of $GdBaCo_{2-x}Ni_xO_{5.5}$. This is surprising since there are extra e_g electrons due to Ni addition much like what is present in oxygen-deficient $GdBaCo_2O_{5.5}$ in the electron doped regime, where a remarkable change in sign of thermopower was observed at 100 K.[31]

Apart from changes in T_{MIT} with Ni substitution, very strong shifts are seen in T_C and T_N as a function of Ni substitution. The variation of all the three transition temperatures with Ni substitution fraction is shown in Fig. 11. This defines the phase diagram as a function of Ni substitution. It can be seen from Fig. 11 that the T_{MIT} obtained from resistivity and DSC are in good agreement with each other. Further, we see that ferromagnetic transition temperatures determined from magnetization and ac susceptibility are also consistent with each other. It is clear from the figure that the variation of the T_{MIT} and T_C with Ni substitution is very similar. To understand this similarity, we recall that electron occupation of the e_g levels in the Co-O_6 octahedra could promote a ferromagnetic exchange between the pyramidal chains.[28] A decrease in crystal field energy, suggested by decrease in T_{MIT} with Ni substitution, could result in the electron occupation of the e_g levels at a lower temperature which, in turn, can stabilize the ferromagnetic interaction at a lower temperature. This can account for T_{MIT} and T_C tracking one another with increase in Ni fraction.

We now try to reconcile the observations made in the magnetization and MR measurements on the Ni-substituted samples. The magnetization data (cf. Fig. 3) indicate that the antiferromagnetic phase is present only for samples with Ni fraction up to $x=0.10$, and that for $x \geqslant 0.20$, a ferromagnetic behavior is seen up to the lowest of temperatures. Large MR was seen for sample with Ni fractions up to $x=0.10$, and moderate MR that increases gradually with decrease in temperature is seen for $x=0.20$ and $x=0.30$ samples. Since MR in this system is associated with the transformation of the AFM phase to a FM phase in the presence of magnetic field, a natural explanation for this observation is that the $x=0.20$ and $x=0.30$ samples contain an admixture of the FM and AFM phases. In the $x=0.40$ sample, no MR is seen but the magnetization curve shows a ferromagnetic behavior, so it can be surmised that for this composition, the sample stabilizes in a FM state.

Before comparing Fig. 11 with the phase diagram proposed as a function of oxygen stoichiometry δ in $GdBaCo_2O_{5+\delta}$,[30] it should be emphasized that in our case, $\delta=0.5$ for all Ni substitutions. Since by replacing Co with Ni we add an electron to the system, Ni substitution without changing oxygen stoichiometry is equivalent to the reduction of oxygen below $\delta=0.5$ in pristine $GdBaCo_2O_{5+\delta}$. In the oxygen stoichiometry case for a reduction of δ from 0.5 to 0.1, the T_C is seen to decrease by $\sim$40 K.[30] Whereas from our phase diagram (cf. Fig. 11), we see that T_C reduces by 100 K for a change in Ni fraction of $x=0.4$. This indicates that Ni substitution has a much larger effect on T_C than oxygen stoichiometry has; as a simple charge balance suggests that for each O depleted, two Co^{3+} convert to the Co^{2+} state per f.u., whereas only one electron is added to the f.u. for each Ni atom substituted. The depletion in T_N with Ni sub-

stitution is ~100 K for a change in Ni fraction of 0.1, which is again larger than the variation seen with oxygen deficiency. Phase coexistence of the antiferromagnetic insulator and ferromagnetic insulator is also seen for $\delta < 0.4$ in the phase diagram proposed by Taskin *et al.*,[30] much like what is seen in the case of Ni substitution shown in Fig. 11. The unusual feature of Fig. 11 is, however, the stabilization of a ferromagnetic phase at low temperatures for high Ni concentrations. Such a ferromagnetic phase is not seen for large oxygen deficiencies in the phase diagram proposed by Taskin *et al.*[30]

V. SUMMARY AND CONCLUSIONS

Substitution of Ni in $GdBaCo_{2-x}Ni_xO_{5.5}$ results in the reduction of the metal-insulator transition temperature T_{MIT}. This seems to be correlated to the orthorhombic distortion observed with Ni substitution. The variation in the ferromagnetic transition temperature with Ni substitution tracks the variation seen in the T_{MIT}. These results indicate that changes in electronic structure induced by Ni substitution govern the T_{MIT} and T_C temperatures. Magnetic field favors a ferromagnetic alignment of the spins on the pyramidal chains, which, in turn, requires the population of the e_g electron in the octahedra. These extra e_g electrons in the octahedra can contribute to an increased conductivity and therefore give rise to the increased negative magnetoresistance in the Ni-substituted samples. The absence of metallization even with a large degree of Ni substitution is in agreement with the suggestion of spin blockade to electron transport seen in the electron doped regime in this system.[29,30]

ACKNOWLEDGMENTS

We thank Shri. V. S. Sastry of Materials Science Division, IGCAR, Kalpakkam for XRD data. We are also indebted to K. Conder, Laboratory for Developments and methods, Switzerland, for clarifications in the oxygen stoichiometry determination.

*Corresponding author.

[1] J. G. Bednorz and K. A. Muller, Z. Phys. B: Condens. Matter **64**, 189 (1986).
[2] M. K. Wu, J. R. Ashburn, C. J. Torng, P. H. Hor, R. L. Meng, L. Gao, Z. J. Huang, Y. Q. Wang, and C. W. Chu, Phys. Rev. Lett. **58**, 908 (1987).
[3] N. F. Mott, *Metal-Insulator Transition* (Taylor & Francis, London, 1990).
[4] M. Imada, A. Fujimori, and Y. Tokura, Rev. Mod. Phys. **70**, 1039 (1998).
[5] R. M. Kusters, J. Singleton, D. A. Keen, R. McGreevy, and W. Hayes, Physica B **155**, 362 (1989).
[6] K. Takeda, H. Sakurai, E. Takayama-Muromachi, F. Izumi, R. A. Dilanian, and T. Sasaki, Nature (London) **422**, 53 (2003).
[7] I. Terasaki, Y. Sasago, and K. Uchinokura, Phys. Rev. B **56**, R12685 (1997).
[8] K. Fujita, T. Mochida, and K. Nakamura, Jpn. J. Appl. Phys., Part 1 **40**, 4644 (2001).
[9] D. Hammer, J. Wu, and C. Leighton, Phys. Rev. B **69**, 134407 (2004).
[10] S. Sugano, Y. Tanabe, and H. Kamimura, *Multiples of Transition: Metal Ions in Crystals* (Academic, New York, 1970).
[11] K. Asai, P. Gehring, H. Chou, and G. Shirane, Phys. Rev. B **40**, 10982 (1989).
[12] P. M. Raccah and J. B. Goodenough, Phys. Rev. **155**, 932 (1967).
[13] M. Zhuang, W. Zhang, and N. Ming, Phys. Rev. B **57**, 10705 (1998).
[14] M. A. Korotin, S. Y. Ezhov, I. V. Solovyev, V. I. Anisimov, D. I. Khomskii, and G. A. Sawatzky, Phys. Rev. B **54**, 5309 (1996).
[15] M. A. Senaris-Rodriguez and J. B. Goodenough, J. Solid State Chem. **116**, 224 (1995).
[16] C. Martin, A. Maignan, D. Pelloquin, N. Nguyen, and B. Raveau, Appl. Phys. Lett. **71**, 1421 (1997).
[17] I. O. Troyanchuk, N. V. Kasper, D. D. Khalyavin, H. Szymczak, R. Szymczak, and M. Baran, Phys. Rev. Lett. **80**, 3380 (1998).
[18] I. O. Troyanchuk, N. V. Kasper, D. D. Khalyavin, H. Szymczak, R. Szymczak, and M. Baran, Phys. Rev. B **58**, 2418 (1998).
[19] A. Maignan, C. Martin, D. Pelloquin, N. Nguyen, and B. Raveau, J. Solid State Chem. **142**, 247 (1999).
[20] Y. Moritomo, M. Takeo, X. J. Liu, T. Akimoto, and A. Nakamura, Phys. Rev. B **58**, R13334 (1998).
[21] E. Suard, F. Fauth, and V. Caignaert, Physica B **276-278**, 254 (2000).
[22] T. Vogt, P. M. Woodward, P. Karen, B. A. Hunter, P. Henning, and A. R. Moodenbaugh, Phys. Rev. Lett. **84**, 2969 (2000).
[23] E. Suard, F. Fauth, V. Caignaert, I. Mirebeau, and G. Baldinozzi, Phys. Rev. B **61**, R11871 (2000).
[24] Y. Moritomo, T. Akimoto, M. Takeo, A. Machida, E. Nishibori, M. Takata, M. Sakata, K. Ohoyama, and A. Nakamura, Phys. Rev. B **61**, R13325 (2000).
[25] W. S. Kim, E. O. Chi, H. S. Choi, N. H. Hur, S.-J. Oh, and H.-C. Ri, Solid State Commun. **116**, 609 (2000).
[26] A. A. Taskin and Yoichi Ando, Phys. Rev. Lett. **95**, 176603 (2005).
[27] C. Frontera, J. L. Garcia-Munoz, A. Llobet, and M. A. G. Aranda, Phys. Rev. B **65**, 180405(R) (2002).
[28] A. A. Taskin, A. N. Lavrov, and Yoichi Ando, Phys. Rev. Lett. **90**, 227201 (2003).
[29] A. Maignan, V. Caignaert, B. Raveau, D. Khomskii, and G. Sawatzky, Phys. Rev. Lett. **93**, 026401 (2004).
[30] A. A. Taskin, A. N. Lavrov, and Yoichi Ando, Phys. Rev. B **71**, 134414 (2005).
[31] A. A. Taskin, A. N. Lavrov, and Y. Ando, Phys. Rev. B **73**, 121101(R) (2006).
[32] E. Pomjakushina, K. Conder, and V. Pomjakushin, Phys. Rev. B **73**, 113105 (2006).
[33] K. Conder, E. Pomjakushina, V. Pomjakushin, M. Stingaciu, S. Streule, and A. Podlesnyak, J. Phys.: Condens. Matter **17**, 5815 (2005).
[34] H. Wu, J. Phys.: Condens. Matter **15**, 503 (2003).

[35] K. Conder, E. Pomjakushina, A. Soldatov, and E. Miltberg, Mater. Res. Bull. **40**, 257 (2005).

[36] R. Nagendran, N. Thirumurugan, M. P. Janawadkar, R. Baskaran, L. S. Vaidhyanathan, A. Bharathi, and Y. Hariharan, AIP Proceedings of the International Conference on Magnetic Materials (AIP, New York, 2007).

[37] P. Yasodha, V. Sridharan, V. Srihari, A. Bharathi, V. S. Sastry, Y. Hariharan, and C. S. Sundar, Solid State Phys. **51**, 719 (2006).